An Investigation of Striplines and Fin Lines with Periodic Stubs

TOSHIHIDE KITAZAWA AND RAJ MITTRA, FELLOW, IEEE

Abstract—**In this paper, a technique based on the network-analytical formalism of electromagnetic fields is used to analyze the strip and fin lines with periodic stubs. Numerical results for the dispersion characteristics of the periodically loaded lines are presented. The effect of the loading stubs on the passband and stopband characteristics is investigated.**

I. Introduction

PROPAGATION characteristics of planar transmission lines for microwave and millimeter-wave integrated circuits have been investigated in the past by many authors. Two of the frequently used transmission media in the microwave frequency range are the strip- and slotlines, while the fin line is known to find applications in the millimeter-wave range. Hybrid-mode analyses of uniform lines of the above types have been reported in the literature [1]–[3]. The periodic-loaded version of these lines finds useful applications in many devices, such as filters [4], [5].

In this paper, an approach for analyzing periodically loaded striplines and fin lines is presented. The network-analytical method is employed to formulate an integral equation for the unknown electromagnetic fields [3] and Galerkin's procedure is used to derive a numerical solution of this equation. The discontinuous-type basis functions, which are similar to those employed in certain open-region scattering problems [6], [7] are used to represent the discontinuity in the aperture field, or the current, at a junction. Numerical results present the passband and stopband properties.

II. The Network Formulation of the Problem

In this section, we illustrate the network-analytical method of formulation by analyzing the problem of fin lines with periodic stubs (see Fig. 1(a)), although the method itself is applicable to the stripline configuration (Fig. (1(b)). The numerical results for both cases will be presented in the next section.

As a first step, we express the transverse (to z) fields in each region by using the Fourier transformation in the x-direction and Floquet harmonic representation in the y-direction as follows:

$$\left.\begin{matrix} E_t^{(i)}(x,y,z) \\ H_t^{(i)}(x,y,z) \end{matrix}\right\} = \sum_{l=1}^{2}\sum_{m=0}^{\infty}\sum_{n=-\infty}^{\infty} \begin{cases} V_{lmn}^{(i)}(z)\, e_{lmn}(x,y) \\ I_{lmn}^{(i)}(z)\, h_{lmn}(x,y), \end{cases} \quad i=1,2,3 \quad \text{(regions)} \tag{1}$$

where

$$e_{1mn}(x,y) = \sqrt{\frac{\eta_m}{2Ap}}\,\frac{1}{K}\{x_0\gamma_m \cos\gamma_m(x+A) - y_0 j\beta_n \sin\gamma_m(x+A)\}\, e^{-j\beta_n y}$$

$$e_{2mn}(x,y) = \sqrt{\frac{\eta_m}{2Ap}}\,\frac{1}{K}\{x_0 j\beta_n \cos\gamma_m(x+A) - y_0\gamma_m \sin\gamma_m(x+A)\}\, e^{-j\beta_n y}$$

$$h_{lmn}(x,y) = z_0 \times e_{lmn}(x,y) \qquad (l=1,2)$$

$$K^2 = \gamma_m^2 + \beta_n^2, \qquad \gamma_m = \frac{m\pi}{2A}, \qquad \beta_n = \beta_0 + \frac{2n\pi}{p}$$

$$\eta_m = \begin{cases} 1 & (m=0) \\ 2 & (m\neq 0) \end{cases} \quad \text{Neumann's number.} \tag{2}$$

Here β_0 is the propagation constant of the dominant harmonic in the Floquet representation, and the vector mode functions e_{lmn}, h_{lmn} satisfy the boundary conditions at $x = \pm A$ as well as the following orthonormal properties:

$$\int_{-A}^{A}\int_{-P/2}^{P/2} e_{lmn}(x,y)\cdot e_{l'm'n'}^{*}(x,y)\, dx\, dy = \delta_{ll'}\delta_{mm'}\delta_{nn'} \tag{3}$$

where $\delta_{ll'}$ is Kronecker's delta and the symbol $*$ signifies complex conjugate. Substituting (1) into Maxwell's field equations and applying the orthonormal properties (3), we obtain the differential equations for $V_{lmn}^{(i)}$ and $I_{lmn}^{(i)}$:

$$\begin{cases} -\dfrac{dV_{lmn}^{(i)}}{dz} = j\kappa_{mn}^{(i)} z_{lmn}^{(i)} I_{lmn}^{(i)} \\ -\dfrac{dI_{lmn}^{(i)}}{dz} = j\kappa_{mn}^{(i)} y_{lmn}^{(i)} V_{lmn}^{(i)} \end{cases} \tag{4}$$

where

$$z_{1mn}^{(i)} = \frac{\kappa_{mn}^{(i)}}{\omega\epsilon_0\epsilon_r^{(i)}}, \qquad z_{2mn}^{(i)} = \frac{\omega\mu_0}{\kappa_{mn}^{(i)}}$$

$$y_{lmn}^{(i)} = \frac{1}{Z_{lmn}^{(i)}}, \qquad \kappa_{mn}^{(i)} = \sqrt{k^2\epsilon_r^{(i)} - K^2}$$

$$k = \omega\sqrt{\epsilon_0\mu_0}, \qquad \epsilon_r^{(i)} = \begin{cases} \epsilon_r & \text{(region (2))} \\ 1 & \text{(otherwise).} \end{cases} \tag{5}$$

Manuscript received September 15, 1983; revised February 21, 1984. This work was partially supported by DAAG29-82-K-0084 and by the Joint Services Electronics Program under Contract JSEP N000-1479C-0424.

T. Kitazawa is with the Electromagnetics Laboratory, University of Illinois, Urbana, IL 61801-2991, on leave of absence from the Kitami Institute of Technology, Kitami Japan.

R. Mittra is with the Electromagnetics Laboratory, University of Illinois, Urbana, IL 61801-2991.

0018-9480/84/0700-0684$01.00 ©1984 IEEE

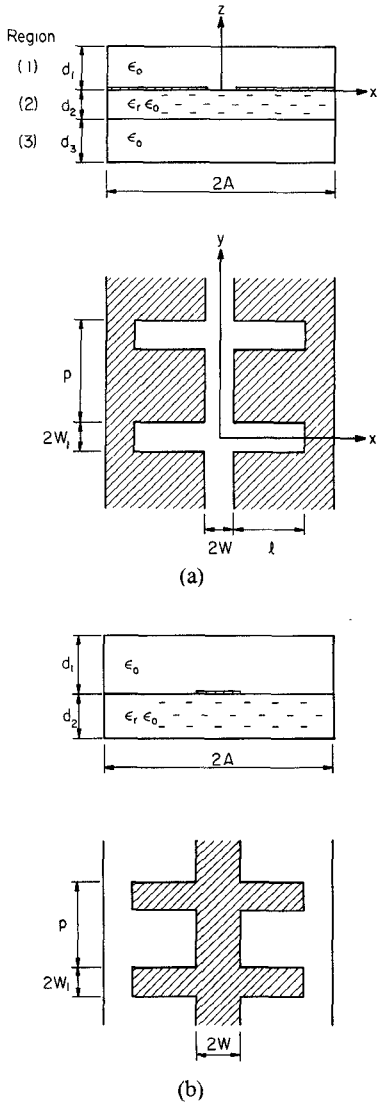

Fig. 1. Planar transmission lines with stubs (a) periodic-loaded fin line, (b) periodic-loaded stripline.

The boundary conditions to be satisfied are expressed as follows:

$$V_{lmn}^{(1)}(d_1) = 0 \tag{6}$$

$$V_{lmn}^{(1)}(+0) = V_{lmn}^{(2)}(-0) = v_{lmn} \tag{7}$$

$$V_{lmn}^{(2)}(-d_2+0) = V_{lmn}^{(3)}(-d_2-0) \tag{8a}$$

$$I_{lmn}^{(2)}(-d_2+0) = I_{lmn}^{(3)}(-d_2-0) \tag{8b}$$

$$V_{lmn}^{(3)}(-d_2-d_3) = 0 \tag{9}$$

and

$$H_t^{(1)}(x, y, +0) = H_t^{(2)}(x, y, -0) \quad \text{(in the aperture of } z=0) \tag{10}$$

where

$$v_{lmn} = \int_{-A}^{A}\int_{-P/2}^{P/2} e_{lmn}^{*}(x', y')\cdot\epsilon(x', y')\,dx'\,dy' \tag{11}$$

and $\epsilon(x, y)$ is the transverse electric field in the aperture at $z = 0$.

Solution of the differential equations (4) and imposition of the boundary conditions (6)–(9) yield the unknowns $V_{lmn}^{(i)}$ and $I_{lmn}^{(i)}$ in each region. The electromagnetic fields, in turn, can be obtained by substituting $V_{lmn}^{(i)}$ and $I_{lmn}^{(i)}$ into (1). Finally, applying the remaining boundary conditions (10), we may obtain the integral equation for the aperture field $\epsilon(x, y)$, and implicitly for the unknown propagation constant β_0:

$$\sum_m\sum_n \int_{-A}^{A}\int_{-P/2}^{P/2} \{Y_{1mn}h_{1mn}(x, y)e_{1mn}^{*}(x', y') + Y_{2mn}h_{2mn}(x, y)e_{2mn}^{*}(x', y')\} \cdot\epsilon(x', y')\,dx'\,dy' = 0 \tag{12}$$

where (x, y) lies in the aperture at $z = 0$ and

$$Y_{1mn} = \omega\epsilon_0\left\{\frac{1}{\kappa_{mn}^{(1)}}\cot(\kappa_{mn}^{(1)}d_1) + \frac{\epsilon_r}{\kappa_{mn}^{(2)}}\frac{\kappa_{mn}^{(2)} - \epsilon_r\kappa_{mn}^{(3)}\tan(\kappa_{mn}^{(2)}d_2)\tan(\kappa_{mn}^{(3)}d_3)}{\kappa_{mn}^{(2)}\tan(\kappa_{mn}^{(2)}d_2) + \epsilon_r\kappa_{mn}^{(3)}\tan(\kappa_{mn}^{(3)}d_3)}\right\}$$

$$Y_{2mn} = \frac{1}{\omega\mu_0}\left\{\kappa_{mn}^{(1)}\cot(\kappa_{mn}^{(1)}d_1) + \kappa_{mn}^{(2)}\frac{\frac{1}{\kappa_{mn}^{(2)}} - \frac{1}{\kappa_{mn}^{(3)}}\tan(\kappa_{mn}^{(2)}d_2)\tan(\kappa_{mn}^{(3)}d_3)}{\frac{1}{\kappa_{mn}^{(2)}}\tan(\kappa^{(2)}d_2) + \frac{1}{\kappa_{mn}^{(3)}}\tan(\kappa_{mn}^{(3)}d_3)}\right\}. \tag{13}$$

The formulation is rigorous up to this stage. The numerical computation for the above equation is explained in the next section.

III. Numerical Computation and Results

Equation (12) can be expressed in an operator form as

$$\bar{\bar{F}}(x, y|x', y')\cdot\epsilon(x', y') = 0 \tag{14}$$

where the dyadic operator $\bar{\bar{F}}\cdot$ is given by

$$\bar{\bar{F}}(x, y|x', y')\cdot = \sum_m\sum_n \int_{-A}^{A}\int_{-P/2}^{P/2} \{Y_{1mn}h_{1mn}(x, y)e_{1mn}^{*}(x', y') + Y_{2mn}h_{2mn}(x, y)e_{2mn}^{*}(x', y')\}\,dx'\,dy'. \tag{15}$$

The determinantal equation for the dispersion relation can be obtained by applying Galerkin's procedure to (14). In this procedure, the unknown aperture field $\epsilon(x, y)$ is expanded in terms of the appropriate basis functions $f_k(x, y)$ as follows:

$$\epsilon(x, y) = \sum_{k=1}^{N} a_k f_k(x, y) \tag{16}$$

where a_k are the unknown coefficients. Substituting (16)

into (14), using $f_m^*(x, y)$ as test functions and taking inner products, we obtain a set of simultaneous equations for the unknown coefficients a_k:

$$[M][a] = 0. \tag{17a}$$

That is

$$\begin{bmatrix} M_{11} & M_{12} & \cdots & M_{1N} \\ M_{21} & & & \\ & \ddots & & \\ \vdots & & & \\ M_{N1} & & & M_{NN} \end{bmatrix} \begin{bmatrix} a_1 \\ a_2 \\ \vdots \\ a_N \end{bmatrix} = 0 \tag{17b}$$

where

$$M_{mk} = \int_{-A}^{A} \int_{-P/2}^{P/2} Z_0 \times f_m^*(x, y) \cdot \left\{ \bar{\bar{F}}(x, y|x', y') \cdot f_k(x', y') \right\} dx\,dy. \tag{18}$$

The determinantal equation for the propagation constant β_0 can be obtained by setting the determinant of the coefficient matrix of (17) equal to zero, i.e.,

$$\det[M(\beta_0)] = 0. \tag{19}$$

It remains only to select the basis functions $f_k(x, y)$. Before defining the basis functions, we introduce three auxiliary functions:

$$S_1(x, y) = \begin{cases} 1 & \left(|x| \leqslant W \text{ and } |y| \leqslant \dfrac{P}{2}\right) \\ 0 & \text{(otherwise)} \end{cases}$$

$$S_2(x, y) = \begin{cases} 1 & \left(|x| \leqslant W \text{ and } W_1 \leqslant |y| \leqslant \dfrac{P}{2}\right) \\ 0 & \text{(otherwise)} \end{cases}$$

$$S_3(x, y) = \begin{cases} 1 & (W \leqslant |x| \leqslant W + l \text{ and } |y| \leqslant W_1) \\ 0 & \text{(otherwise)}. \end{cases} \tag{20}$$

The regions represented by these functions are shown in Fig. 2. The basis functions to be used are defined by employing these auxiliary functions:

$$f_1(x, y) = x_0 X(x) e^{-j\beta_0 y} S_1(x, y) \tag{21a}$$

$$f_2(x, y) = x_0 X(x) e^{-j\beta_{-1} y} S_1(x, y) \tag{21b}$$

$$f_3(x, y) = x_0 \operatorname{sgn}(y) X(x) e^{-j\beta_0 y} S_2(x, y) + y_0 \operatorname{sgn}(x) \cos\left\{\frac{\pi}{2(l+W)} x\right\} Y(y) S_3(x, y) \tag{21c}$$

$$f_4(x, y) = x_0 \operatorname{sgn}(y) X(x) e^{-j\beta_{-1} y} S_2(x, y) + y_0 \operatorname{sgn}(x) \cos\left\{\frac{\pi}{2(l+W)} x\right\} Y(y) S_3(x, y) \tag{21d}$$

where

$$\beta_{-1} = \beta_0 - \frac{2\pi}{p}$$

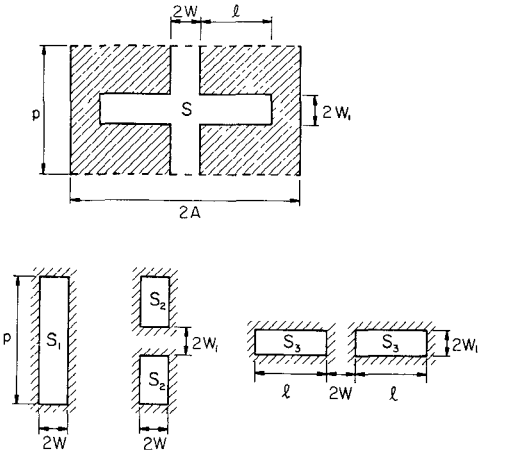

Fig. 2. Regions represented by (20).

and $X(x)$ and $Y(y)$ represent the x- and y-variations in the main- and stub-fin lines, respectively. Three different functions were tested for $X(x)$ and $Y(y)$, viz.,

(i) $X(x) = \dfrac{C}{W}$ $Y(y) = \dfrac{C}{W_1}$, C: constant

(ii) $X(x) = \dfrac{|x|}{W}$ $Y(y) = \dfrac{|y|}{W_1}$

(iii) $X(x) = \dfrac{1}{W}\left\{1 + \left|\dfrac{x}{W}\right|^3\right\}$ $Y(y) = \dfrac{1}{W_1}\left\{1 + \left|\dfrac{y}{W_1}\right|^3\right\}$. (22)

We mention that the functions in (21c) and (21d) are quite similar in character to the junction basis functions that have been employed in scattering problems [6], [7], together with $X(x)$ and $Y(y)$ given by (i) in (22) and have been found to yield good results for these open-region problems. However, for the transmission-line calculations, where the near-field is important, computations have been carried out [8], [9] using the basis functions given in (ii) and (iii) in (22).

Fig. 3 shows the $k - \beta_0$ diagram for a fin line with periodic stubs. Computations were performed for three different sets of basis functions given in (22), but the differences were found to be rather small. However, the basis functions given in (iii) have been employed for the computations in this paper because of superior convergence properties without undue increase in computation time. The curve for the periodically loaded fin line (solid line) is lower than for the uniform fin line without stubs (broken line) because of the inductive reactance of the series stubs. The passband and stopband regions, which are common in the dispersion diagrams in periodic structures [10] and are applicable to filters, are clearly evident in Fig. 3. The first passband occurs in the frequency range when kp satisfies $1.038 < kp < 2.800$ and the first stopband $2.800 < kp < 2.931$. It should be noted that the higher order stopbands will appear in the higher frequency range; however, since the higher order (even) mode of the uniform fin line (without stubs) can propagate in the range $kp > 4.315$, these higher stopbands have little significance.

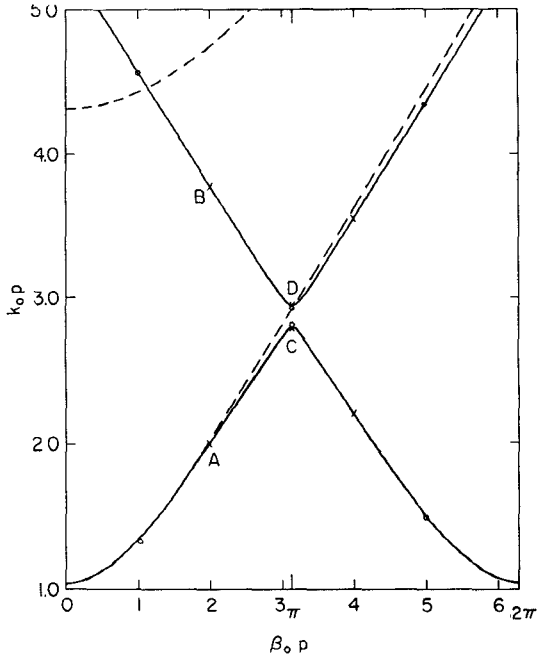

Fig. 3. The $k-\beta_0$ diagram for a periodic-loaded fin line. $\epsilon_r = 2.2$, $d_1 = 0.094$ in, $d_2 = 0.005$ in, $d_3 = 0.089$ in, $W = 0.0025$ in, $A = 0.047$ in, $W_1 = 0.01$ in, $l = 0.04$ in, $p = 0.12$ in, ------ uniform fin line. Fin line with stubs using $X(x)$ and $Y(y)$ given in: ∘ ∘ (i) in (22), × × (ii) in (22), — — — (iii) in (22).

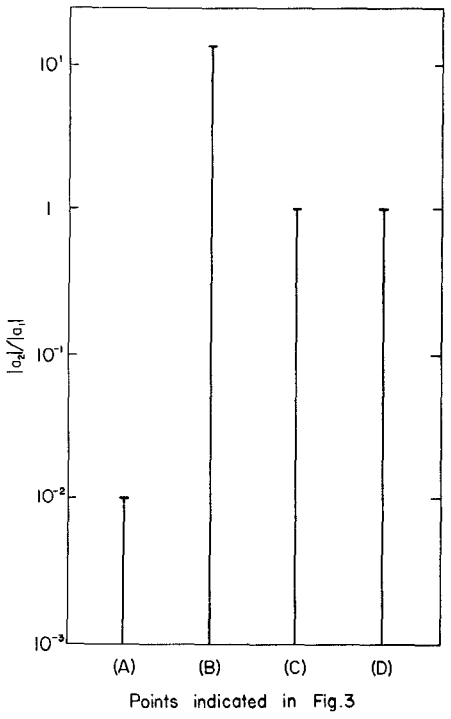

Fig. 4. The relative amplitude of coefficients of basis functions f_1 and f_2.

Fig. 4 shows the relative amplitude of the coefficients of basis functions f_1 and f_2, which represent the $n = 0$ and $n = -1$ harmonics, respectively, at each point indicated in Fig. 3. These results show that the first stopband is caused by the coupling between the $n = 0$ and $n = -1$ harmonics.

Fig. 5 shows the effect of the loading stubs on the normalized stopband width $\Delta k/k_c$, where Δk is the stopband width and k_c is the center frequency. The stub length l is smaller than the quarter wavelength of the stub fin line, so the series stubs have an inductive reactance; therefore, the longer the stub, the wider the stopband. The characteristic impedance of the fin line becomes larger as the gap becomes wider [2]; therefore, the stopband becomes wider with wider stubs, although the dependence on the stub width is relatively small.

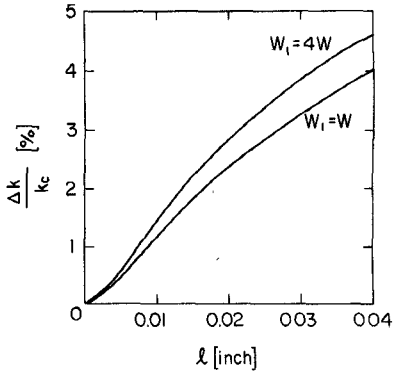

Fig. 5. The effect of the loading stubs of the fin line. $\epsilon_r = 2.2$, $d_1 = 0.094$ in, $d_2 = 0.005$ in, $d_3 = 0.089$ in, $W = 0.0025$ in, $A = 0.047$ in, $p = 0.12$ in.

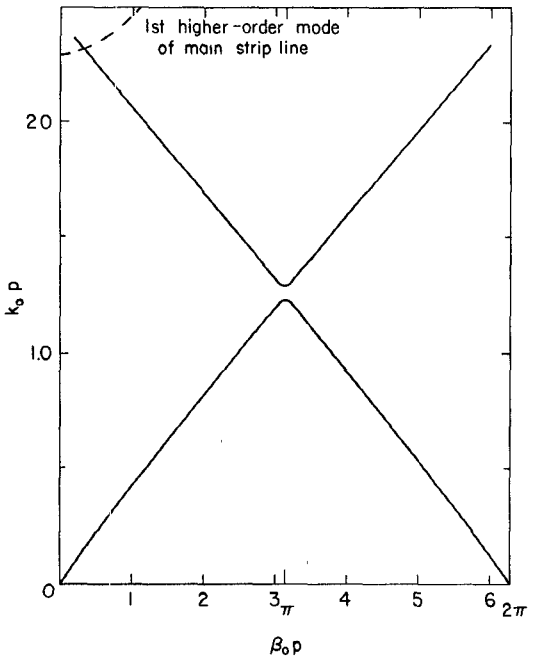

Fig. 6. The $k-\beta_0$ diagram for a periodic-loaded stripline. $\epsilon_r = 8.875$, $d_1 = 11.43$ (mm), $d_2 = 1.27$ (mm), $W = 0.3175$ (mm), $A = 6.35$ (mm), $W_1 = 0.3175$ (mm), $l = 4$ (mm), $p = 10$ (mm).

Fig. 6 shows the $k-\beta_0$ diagram of the stripline with periodic stubs. Again, the passband and stopband properties are observed in this case, with the first passband occurring when $0 < kp < 1.228$ and the first stopband when $1.228 < kp < 1.286$. The first higher order mode of the main stripline appears when $kp = 2.289$; therefore, the higher order stopbands have no meaning in the same way as the case of fin line.

Fig. 7 shows the effect of the loading stubs. The characteristic impedance of the stripline becomes smaller as the strip becomes wider [3], but the stubs are shunt-connected

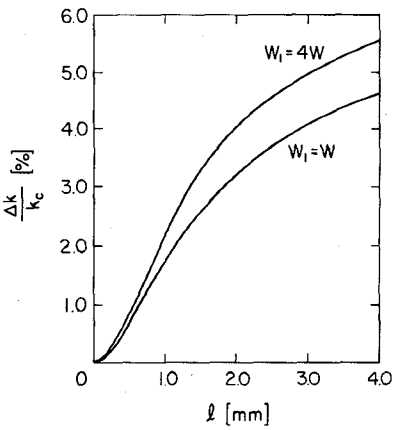

Fig. 7. The effect of the loading stubs of the stripline. $\epsilon_r = 8.875$, $d_1 = 11.43$ (mm), $d_2 = 1.27$ (mm), $W = 0.3175$ (mm), $A = 6.35$ (mm), $p = 10$ (mm).

in this case. Therefore, the stopband, again, becomes wider with wider stubs.

IV. Conclusions

A method of analysis for the stripline and the fin line with periodic stubs has been presented, and the $k - \beta_0$ diagrams for these structures have been computed. It is found that the passband and stopband properties are generated from the coupling between the $n = 0$ and $n = -1$ harmonics. The effects of the loading stubs have been determined numerically.

References

[1] G. Kowalski and R. Pregla, "Dispersion characteristics of shielded microstrips with finite thickness," *Arch. Elek. Ubertragung*, vol. 25, pp. 193–196, Apr. 1971.

[2] Y. Hayashi, E. Farr, S. Wilson, and R. Mittra, "Analysis of dominant and higher-order modes in unilateral fin lines," *Arch. Elek. Ubertragung*, vol. 37, pp. 117–122, Mar. 1983.

[3] T. Kitazawa and Y. Hayashi, "Propagation characteristics of strip lines with multilayered anisotropic media," *IEEE Trans. Microwave Theory Tech.*, vol. MTT-31, pp. 429–433, June 1983.

[4] H. Entschladen and H. J. Siweris, "Slot line stub filters," *Arch. Elek. Ubertragung*, vol. 34, pp. 152–156, Apr. 1980.

[5] H. Hofmann, "MM-wave Gunn oscillator with distributed feedback fin-line circuit," presented at the 1980 MTT-S Int. Symp., Washington, DC, 1980.

[6] C. H. Tsao and R. Mittra, "Spectral-domain analysis of frequency selective surfaces (FSS) comprised of periodic arrays of cross-dipoles and Jerusalem-crosses," *IEEE Trans. Antennas Propagat.*, to be published.

[7] H. H. Ohta, K. C. Lang, C. H. Tsao, and R. Mittra, "Frequency selective surface for satellite communications antenna applications," presented at the 1982 AP-S Int. Symp., Albuquerque, NM, 1982.

[8] E. Yamashita and R. Mittra, "Variational method for the analysis of microstrip lines." *IEEE Trans. Microwave Theory Tech.*, vol. MTT-16, pp. 251–256, Apr. 1968.

[9] T. Itoh and R. Mittra, "A technique for computing dispersion characteristics of shielded microstrip lines," *IEEE Trans. Microwave Theory Tech.*, vol. MTT-22, pp. 896–898, Oct. 1974.

[10] R. E. Collin, *Field Theory of Guided Waves*. New York: McGraw-Hill, 1960, p. 368.

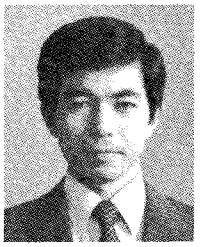

Toshihide Kitazawa was born in Sapporo, Japan, on December 1, 1949. He received the B.E., M.E., and D.E. degrees in electronics engineering from Hokkaido University, Sapporo, Japan, in 1972, 1974, and 1977, respectively.

He was a Post-Doctoral Fellow of the Japan Society for the Promotion of Science from 1979 to 1980. Since 1980, he has been an Associate Professor of Electronic Engineering at the Kitami Institute of Technology, Kitami, Japan. Currently, he is a Visiting Assistant Professor of Electrical Engineering at the University of Illinois, Urbana.

Dr. Kitazawa is a member of the Institute of Electronics and Communication Engineers of Japan.

Raj Mittra (S'54–M'57–SM'69–F'71) is Professor of Electrical Engineering and Associate Director of the Electromagnetics Laboratory at the University of Illinois in Urbana. He serves as a Consultant to several industrial and governmental organizations, including the NASA Jet Propulsion Laboratory of the California Institute of Technology.

His professional interests include the areas of analytical and computerated electromagnetics, satellite antennas, integrated circuits, coherent optics, transient problems, radar scattering, etc. He is Past-President of the IEEE Antennas and Propagation Society (AP-S), is past Editor of the *IEEE Transactions on Antennas and Propagation*, and is an active contributor to many activities of the AP-S.